Tailored Formation of N-Doped Nanoarchitectures by Diffusion-Controlled on-Surface (Cyclo)-Dehydrogenation of Heteroaromatics

Anna Lisa Pinardi,[†] Gonzalo Otero-Irurueta,[†] Irene Palacio,[†] Jose Ignacio Martinez,[†] Carlos Sanchez-Sanchez,[†] Marta Tello,[†] Celia Rogero,[‡] Albano Cossaro,[§] Alexei Preobrajenski,[⊥] Berta Gómez-Lor,[†] Andrej Jancarik,[∥] Irena G. Stará,[∥] Ivo Starý,[∥] M. Francisca Lopez,[†] Javier Méndez,[†] and Jose Angel Martin-Gago[†,#,*]

[†]Instituto de Ciencia de Materiales de Madrid ((ICMM), Consejo Superior de Investigaciones Científicas (CSIC), Sor Juana Inés de la Cruz 3, Cantoblanco, 28049 Madrid, Spain, [‡]Centro de Física de Materiales (CSIC-UPV/EHU), Materials Physics Center (MPC), Donostia International Physics Center (DIPC), 20018, San Sebastian, Spain, [§]CNR-IOM, Laboratorio TASC, Basovizza SS-14, Km 163.5, I-34149 Trieste, Italy, [⊥]MAX-IV Laboratory, Lund University, Box 118, 22100 Lund, Sweden, [∥]Institute of Organic Chemistry and Biochemistry, Academy of Sciences of the Czech Republic, Flemingovo nám. 2, 16610 Prague 6, Czech Republic, and [#]Centro de Astrobiología (CSIC-INTA), Carretera de Torrejón a Ajalvir, km 4, 28850 Torrejón de Ardoz, Madrid, Spain. A.L.P. conducted all UHV experiments. STM experiments on different samples were also performed by G.O.-I., M.T., C.S.-S., and C.R. Synchrotron radiation measurements were assisted by I.P., A.P., and A.C. Calculations were performed by J.I.M. Organic precursors were designed and fabricated by A.J., B.G.-L., I.S., and I.G.S. Experiments were conceived and designed by M.F.L., J.M., I.S., I.G.S., and J.A.M.-G, and they co-wrote the manuscript. J.A.M.-G. coordinated the whole research. All authors discussed the results and commented on the manuscript.
Present address: Carlos Sanchez-Sanchez: Empa. Swiss Federal Laboratories for Materials Science and Technology, Uberlandstrasse 129, 8600 Dübendorf, Switzerland.

ABSTRACT

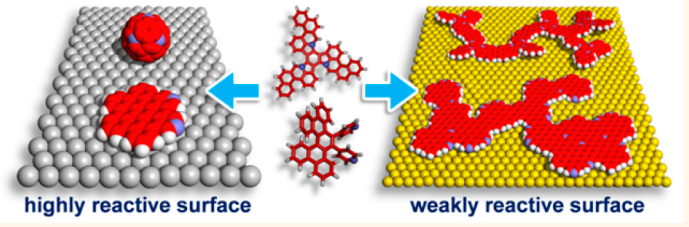

Surface-assisted cyclodehydrogenation and dehydrogenative polymerization of polycyclic (hetero)aromatic hydrocarbons (PAH) are among the most important strategies for bottom-up assembly of new nanostructures from their molecular building blocks. Although diverse compounds have been formed in recent years using this methodology, a limited knowledge on the molecular machinery operating at the nanoscale has prevented a rational control of the reaction outcome. We show that the strength of the PAH−substrate interaction rules the competitive reaction pathways (cyclodehydrogenation *versus* dehydrogenative polymerization). By controlling the diffusion of N-heteroaromatic precursors, the on-surface dehydrogenation can lead to monomolecular triazafullerenes and diazahexabenzocoronenes (N-doped nanographene), to N-doped oligomeric or polymeric networks, or to carbonaceous monolayers. Governing the on-surface dehydrogenation process is a step forward toward the tailored fabrication of molecular 2D nanoarchitectures distinct from graphene and exhibiting new properties of fundamental and technological interest.

KEYWORDS: surface-assisted dehydrogenation · N-doped nanographene · heteroaromatic polymer · STM · surface diffusion · bottom-up assembling

The controlled on-surface formation of intricate π-electron systems may ultimately overcome the limits of the conventional synthesis, which often faces severe problems if large, fragile, or insoluble molecules are to be prepared in solution and subsequently deposited on a solid substrate. Central to such efforts are complex carbon-rich molecules or materials, whose bottom-up synthesis at the nanoscale represents a great challenge today. Molecular architectures featuring π-conjugation are expected to mediate efficient charge transfer, and therefore, they are particularly attractive for future molecular electronics applications. Since the discovery of graphene, significant

* Address correspondence to gago@icmm.csic.es.

Received for review February 8, 2013 and accepted March 19, 2013.

Published online March 19, 2013
10.1021/nn400690e

progress has been made in the top-down approach to its etched or carved fragments.[1] In contrast, on-surface synthesis appears as a key molecular mechanism for controlling bottom-up assembling of new nanostructures.[2] Although this synthetic route is still in its embryonic state, the first breakthroughs have already been reported. Thus, (hetero)fullerenes,[3,4] nanographenes,[5] graphene nanoribbons,[6] polyaromatic domes,[7] aromatic oligomers/polymers, or 2D architectures from suitable precursors have already been achieved. Therefore, upon combining unconventional synthesis issues with a practical methodology, highly attractive π-electron systems on a metal,[3−12] semiconductor, or insulator[13] surface could be available.

The bottom-up approach to new functional nanostructures and two-dimensional (2D) materials should retain the key features of a traditional synthesis but also employ specific phenomena such as on-surface self-assembly and on-surface reactivity of individual molecular components to be covalently interconnected under the outmost control of the reaction outcome. This is particularly important when doping is required to modify the electronic properties of 2D materials, such as graphene. Substitutional doping is a powerful way of tailoring the material properties, and the use of heteroaromatic precursors permits an easy and rational control of the doping in the final reaction outcome.[14]

The emerging on-surface covalent coupling methodology[2,6,8−13,15−23] employs so far a limited portfolio of useful carbon−carbon bond-forming reactions: cyclodehydrogenation (analogous to the Scholl reaction), dehydrogenative oligomerization[20] or polymerization,[22] radical dimerization[24] (analogous to the Ullmann coupling), carbene dimerization,[22] and aryl halide−alkyne coupling[23] (analogous to the Sonogashira reaction). Among these reactions, cyclodehydrogenation (intramolecular oxidative C−C coupling) and dehydrogenative oligo- or polymerization (intermolecular oxidative C−C coupling) are especially attractive. The processes formally correspond to C−H activation of both precursors followed by their (cross)coupling.[2] In particular, the mechanism of cyclodehydrogenation of a polyaromatic precursor and the role of the metal surface were studied experimentally and theoretically in detail for the specific case of Cu(111):[5] cyclodehydrogenation was used to form nanographene following a rational methodology. Within this general frame of coupling reactions by dehydrogenation, we show hereafter that the strength of the surface−adsorbate interaction can promote or restrain diffusion of the precursors and hence control the formation of new tailored nanostructures with different dimensionality (see Figure 1).

Significant progress in this area has been enabled by ultrahigh-vacuum scanning tunneling microscopy (UHV STM), which is a suitable technique for imaging nano-objects with ultimately intramolecular resolution. In this work we combine advanced *in situ* surface characterization techniques as STM, near-edge X-ray adsorption fine structure (NEXAFS), and high-resolution X-ray photoemission spectroscopy (XPS) with theoretical *ab initio* calculations including van der Waals (vdW)

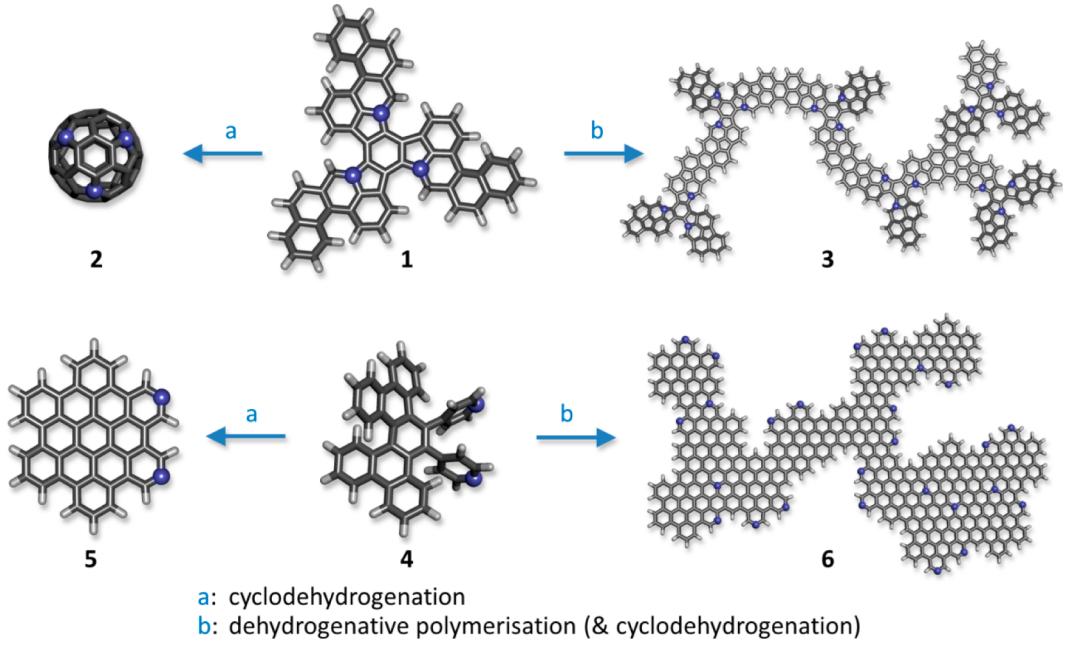

Figure 1. Heteroaromatic precursors 1 and 4 subjected to controlled on-surface dehydrogenation. 1 and 4 may form nitrogen-doped triazafullerene 2 or 2,5-diazahexabenzocoronene 5 (both through intramolecular cyclodehydrogenation) or branched and cross-linked 2D polyaromatic architectures 3 or 6 (both through intermolecular dehydrogenative polymerization accompanied by intramolecular cyclodehydrogenation). Nitrogen atoms are highlighted as blue balls; 3 and 6 represent only conjectural structures.

forces to yield a complete understanding of the self-assembling of molecular precursors on surfaces. Herein, by merging information from these techniques and using different single-crystal metal substrates, we demonstrate an unprecedented diffusion control over competitive intramolecular and intermolecular dehydrogenative processes, called cyclodehydrogenation and dehydrogenative polymerization, respectively, which determine the structure of the product. By following this procedure, we were able to efficiently prepare N-doped fullerene, nanographene, polyaromatic networks, carbonaceous overlayers, or graphene (Figure 1).

RESULTS AND DISCUSSION

Design of the Model Precursors 1 and 4. In order to study the substrate-controlled competition of on-surface cyclodehydrogenation *versus* dehydrogenative polymerization, we have chosen two heteroaromatic precursors, **1** and **4** (Figure 1). The 3-fold symmetric clover-shaped and nearly flat crushed-fullerene precursor **1** ($C_{57}H_{33}N_3$)[26] was already shown to undergo cyclodehydrogenation on single-crystal platinum surfaces, yielding triazafullerene **2** ($C_{57}N_3$) by removing 33 H atoms.[3] The easily accessible[27] pyridyl-substituted dibenzo[5]helicene **4** ($C_{40}H_{24}N_2$; for its synthesis, see Supporting Information) adopts a nonplanar helical conformation that increases its solubility and facilitates its sublimation due to a limited $\pi-\pi$ stacking. Since precursor **4** can undergo full planarization through on-surface cyclodehydrogenation by removing 8 H atoms, 2,5-diazahexabenzocoronene **5** ($C_{40}H_{16}N_2$) can be obtained. Normally, polyaromatic precursors undergo cyclodehydrogenation rather than dehydrogenative polymerization whenever possible due to entropic and steric factors (the loss of hydrogen is expected to occur preferentially at sterically congested sites).[28] However, we propose that under certain reaction conditions the on-surface dehydrogenative polymerization of **1** or **4** can compete with cyclodehydrogenation or even overwhelm it. In this scenario branched and curled nanoribbons or 2D cross-linked polyaromatic network **3** or **6** can be formed on a metal surface.

Cyclodehydrogenation of 1 and 4 on the Pt(111) Surface. We deposited precursors **1** and **4** under UHV conditions on the highly interacting single-crystal Pt(111) surface at room temperature (RT) (Figure 2). At low coverage (*ca.* 0.3 ML), the STM images show individual molecules of **1** (Figure 2a) and **4** (Figure 2c) scattered over the surface with no preferential adsorption at the step edges. This indicates that both precursors are well anchored to their adsorption sites and, accordingly, their diffusion is substantially restricted. However, the molecule–substrate interaction is not strong enough to disrupt the molecular structure.[29] Our calculations reproduce this experimental observation. We have found by density functional theory (DFT) that the precursor **4** adsorbs 0.31 nm above the surface by

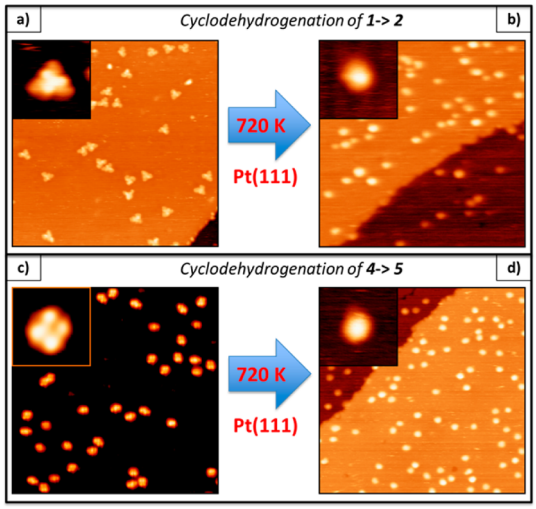

Figure 2. Dehydrogenation of 1 and 4 on the Pt(111) single-crystal surface. UHV STM images of *ca.* 0.3 ML of precursor 1 (a, 30 × 30 nm^2, inset 4 × 4 nm^2, $V_{substrate}$ = +0.5 V) and precursor 4 (c, 30 × 30 nm^2, inset 4 × 4 nm^2, $V_{substrate}$ = +2.0 V) deposited on Pt(111) at room temperature show individual molecules with intramolecular structure corresponding to molecular orbitals. After annealing at 720 K, the cyclodehydrogenation process occurs and 1 is transformed into the spherical triazafullerene 2 (b, 30 × 30 nm^2, inset 4 × 4 nm^2, $V_{substrate}$ = +0.5 V) and 4 is transformed into the flat 2,5-diazahexabenzocoronene 5 (d, 30 × 30 nm^2, inset 4 × 4 nm^2, $V_{substrate}$ = +2.0 V).

electrostatic interactions derived from vdW forces with a binding energy of 1.5 eV per molecule, which is high enough to prevent its diffusion. Moreover, the electrostatic nature of this interaction, and therefore the absence of covalent bonding, does not modify the structure of the molecule as we experimentally observe. We clearly distinguish in the STM images the shape of individual molecules and resolve the submolecular structure of **1** (in agreement with previous studies;[7] Figure 2a, inset) and **4** (Figure 2c, inset).[3,29]

Upon annealing **1** and **4** on Pt(111) at about 720 K, they both change their shape, size, and intramolecular structure (Figure 2b and d). In the case of **1**, its shape converts from triangular to spherical (**2**) (Figure 2b). The transformation of **1** to triazafullerene **2** is accompanied by significant morphological changes: the width decreases from 2.2 nm to 1.2 nm and the apparent height increases from 0.20 nm to 0.45 nm (Figure 2b). These observations are in agreement with related studies on fullerene nanostructures deposited on similarly reactive surfaces.[30] The cyclodehydrogenation of **1** into **2** has been widely described by Otero *et al.*[3] In this work, XPS spectra showed that the nanostructures observed by STM in Figure 2b are made of N and C atomic species with their expected stoichometric ratio for the triazafullerene **2**.

Concerning the precursor **4**, its four-protrusion internal structure disappears upon annealing and rounded features are imaged with the STM (Figure 2d). The lateral size (diameter) changes from 1.7 nm to 1.4 nm

and the apparent height from 0.28 nm to 0.23 nm. These newly formed nanostructures feature a loss of the intramolecular resolution, indicating the formation of N-doped nanographenes **5**. This agrees with previous studies on forming and imaging hexabenzocoronene structures on surfaces,[7,31,32] our own spectroscopic analysis (Figure S5 in the Supporting Information), and the STM image simulation, which demonstrates that STM images of **5** do not show any intramolecular resolution (see Figure S9 in the Supporting Information). Moreover, similarly to the case of **2**, XPS spectra show that the nanostructures observed by STM in Figure 2d are made of N and C atomic species with their expected molecular stoichiometric ratio for **5**.

Curiously, the lateral size estimated by the STM of the pristine molecule decreases as it cyclodehydrogenates and forms N-doped nanographene even though the real width of the molecule does not change remarkably (see Figure 1). The spatial delocalization of the molecular orbitals involved in the tunnel current of the two species is very different. The loss of localized electronic states when going from **4** to **5** results in a width reduction of about 20%.

To obtain further insights into the reaction mechanism, we analyze the intramolecular cyclodehydrogenation of **4** on Pt(111) by means of large-scale *ab initio* simulations accounting for all molecule−surface interactions including vdW forces in a DFT framework within a local density exchange−correlation parametrization (see Supporting Information). This treatment is not restricted to the ground state of the isolated species, but gives detailed insights into intramolecular C−C coupling by explicitly computing reaction barriers to explain the formation of N-doped nanographenes from the heteroaromatic precursor. As a starting point we compute **4** adsorbed on the Pt(111) surface (top and side views sketched in the top panel, step 1, of Figure 3), obtaining a minimum energy structure by locating the precursor at a perpendicular distance of 0.31 nm above the substrate. From this point, and in order to establish a reliable reaction pathway toward the formation of N-doped nanographene **5** from **4** by a cascade of cyclodehydrogenations (sketched in the top panel of Figure 3), we fully optimize the structure of each intermediate on Pt(111), calculating accordingly the energy barriers by means of the nudged elastic band algorithm.[33] On the basis of the C−H bond dissociation propensity (see Supporting Information), we could identify the "*weakest*" C−H bonds in the molecule, while the rest remain unaffected.[5] Thus, a complete reaction scenario can be described as a repetitive sequence of consecutive processes: (i) the thermally induced kinetically controlled removal of a "preselected" hydrogen atom to form a reactive aryl radical (energy barrier of *ca.* 1.5 eV), (ii) the rotation of the respective aromatic ring with a dangling bond toward another proximal "preselected" C−H bond,

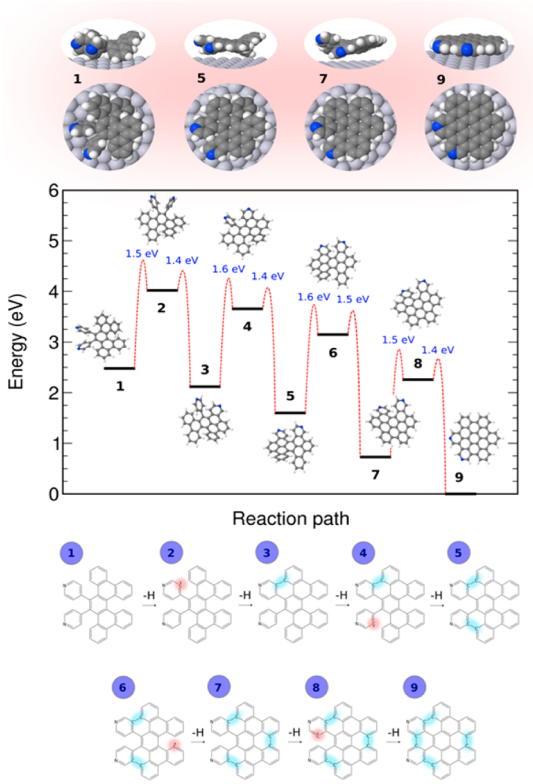

Figure 3. Computed reaction pathway diagram for the cyclodehydrogenation of 4 to 5 on Pt(111) based on *ab initio* calculations. The reaction proceeds *via* seven metastable intermediates (2−8). All energies (in eV) are referred to the final N-doped nanographene reaction product (step 9). Energy barriers (in eV) are shown for each elementary step. Images of the most representative metastable states (1, 5, 7, 9) along the surface-assisted cyclodehydrogenation process are also depicted (top panels). A chemical structure diagram is included (bottom panel) to visually illustrate the different dehydrogenation steps (highlighted in red) and the subsequent C−C bond formations (highlighted in blue).

(iii) the final removal of the second hydrogen atom, and (iv) the radical aromatic addition to create a new C−C bond (energy barrier of 1.4−1.6 eV). With these elementary mechanisms repeated up to four times to complete the formation of four C−C bonds, the full reaction pathway (depicted in Figure 3) exhibits a net energy gain of 2.48 eV in favor of the final N-doped nanographene reaction product.

Dehydrogenation of 1 and 4 on the Au(111) Surface. Intriguingly, we obtained an entirely different picture when changing the platinum substrate to gold (Figure 4). In contrast to Pt(111), the Au(111) single-crystal surface is known to interact weakly with adsorbed aromatics and, accordingly, it is considered to be inert toward some catalytic reactions.[34] Indeed, after the deposition of about 0.4 ML of **1** or **4** on the Au(111) surface at room temperature no molecules are seen by STM because they diffuse faster than the scanning speed (Figure 4a and c, respectively). The presence of **1** and **4** in its molecular form on the surface was corroborated by XPS (see Supporting Information).

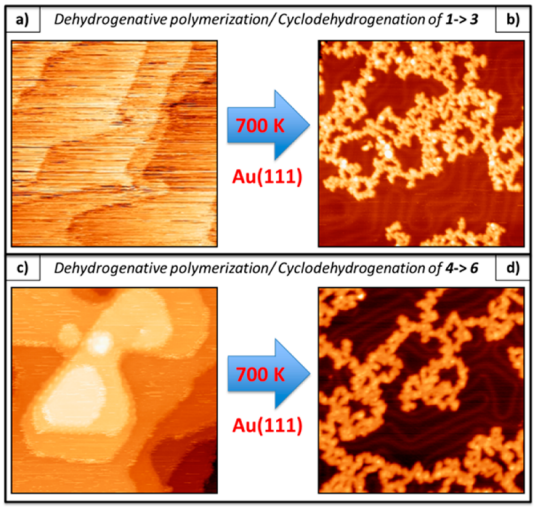

Figure 4. Dehydrogenative polymerization/cyclodehydrogenation of 1 and 4 on the single-crystal Au(111) surface. UHV STM images of *ca.* 0.4 ML of precursor 1 (a, 30 × 30 nm^2, $V_{substrate}$ = +0.5 V) and precursor 4 (c, 30 × 30 nm^2, $V_{substrate}$ = +2.0 V) deposited on Au(111) at room temperature do not show individual molecules. After annealing 1 and 4 at 700 K, the dehydrogenative polymerization/cyclodehydrogenation processes occur and 1 is transformed into the 2D polyaromatic network 3 (b, 40 × 40 nm^2 $V_{substrate}$ = +0.75 V), and similarly 4 to 6 (d, 40 × 40 nm^2, $V_{substrate}$ = +2.0 V).

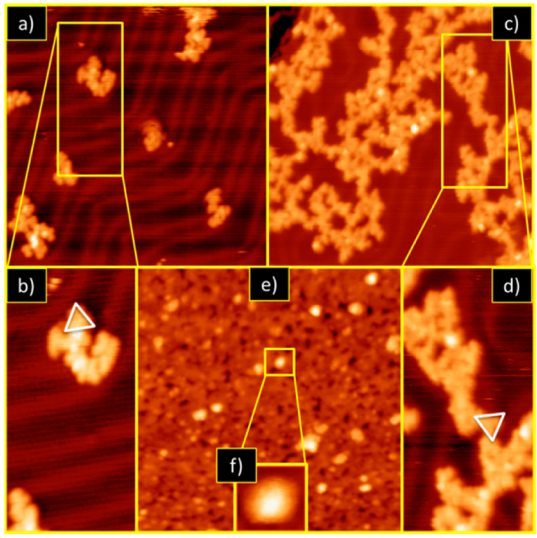

Figure 5. (Cyclo)dehydrogenation of 1 to form new nanoarchitectures with different dimensionality. STM images of 1 deposited on Au(111) at different temperatures and coverage. (a) 0.1 ML at 540 K (30 × 30 nm^2). Small oligomeric clusters nucleate at the corner of the surface reconstruction (formation of 0D nanostructures). (b) Zoom-in of one nanoaggregate (8.5 × 17.2 nm^2). The triangular topology that characterizes 1 can be clearly distinguished (white triangle), indicating partial dehydrogenation. (c) 0.3 ML at 600 K (30 × 30 nm^2). The formation of a linear polymeric network made up of individual molecules indicates a 2D cross-linking of the deposited precursor. (d) Detail of one of the branches of the polymer, where the white triangle indicates the smallest building block (8.5 × 17.2 nm^2). (e) 1 ML at 900 K (40 × 40 nm^2). A N-doped carbon 2D membrane is formed with a series of interlinked partially folded structures. (f) Individual heterofullerenes are observed embedded into the layer in some areas of the image (3 × 3 nm^2). The presence of N in all these nanoarchitectures was confirmed by XPS. Typical bias and tunnel current were 750 mV and 0.1 nA, respectively.

However, upon annealing **1** and **4** to 700 K, we observe the formation of 2D polymeric cross-linked networks **3** and **6** (Figure 4b and d, respectively). The highly diffusing precursors **1** and **4** partially cyclodehydrogenate and dehydrogenate, meet other diffusing (and also dehydrogenated) adsorbed precursors, and covalently bind together. After a few molecules merge *via* dehydrogenative oligomerization, the diffusion of such nanoclusters diminishes. Once these molecular seeds fix on the gold surface, a random network of branched molecules forms since polymerization does not follow any preferential crystallographic direction. In some sections of the network, we can distinguish a triangular or round topology in their constituent units resembling that of the original precursor **1** and **4**, respectively. Indeed, in Figure 4b a few brighter molecules are seen inside the branches, which are related to both partially and/or completely cyclodehydrogenated triazafullerenes.

Figures 2 and 4 demonstrate that surface diffusion is the key mechanism driving cyclodehydrogenation and dehydrogenative polymerization of the same molecular precursor (**1** and **4**) either to the formation of individual nano-objects (**2** and **5**) or to extended networks (**3** and **6**) as schematically represented in Figure 1. The interplay between molecule−surface and molecule−molecule interactions causes the reaction to move toward either the left or the right in Figure 1.

The degree of polymerization of the precursors **1** and **4** and, accordingly, the structure as well as dimensionality of the formed nano-objects depend on the annealing temperature and surface coverage. Indeed, on depositing a lower coverage of **1** (0.1 ML) on Au(111) and annealing to a lower temperature (540 K), small oligomeric clusters **3** become visible by UHV STM as they anchor to the surface at the elbows of the herringbone reconstruction (Figure 5a and b) or at the step edges. High-resolution STM images show that the oligomeric clusters **3** consist of a few covalently bound subunits, some of which retain the triangular shape and molecular orbitals of precursor **1** (Figure 5b), meaning that only partial (cyclo)dehydrogenation of **1** took place, which leads to oligomerization rather than folding. These nanoclusters **3** are weakly bound to the surface since they can be easily moved by the STM tip (see Supporting Information). Interestingly, we have observed that low coverage promotes the formation of small oligomers, whereas coverage close to single layer leads to the formation of polymeric chains and networks.

Upon increasing the activation temperature to 600 K, polymeric chains topologically similar to those presented in Figure 4b and d are formed (Figure 5c,d). However, in a few cases we can still distinguish the intramolecular structure of the original precursor **1**, as indicated by the white triangle in Figure 5d. This shows

that cyclodehydrogenation is not complete at this temperature (see Supporting Information). A few brighter spots are visible in Figure 5c and d. These particular precursors undergo cyclodehydrogenation to a higher degree than the others, and open-cage and/or closed triazafullerenes with a higher apparent height are formed.

In order to favor the dehydrogenation processes and form a complete 2D N-doped carbon monolayer, we increase the coverage to 1 ML and the temperature of the substrate to 900 K. Then, all triangular-shaped substructures disappear and a dense membrane-like structure is formed (Figure 5e). Evidently, an extensive dehydrogenative polymerization took place as a consequence of the high coverage and, at the same time, cyclodehydrogenation proceeded to a higher degree than at 600 K since folded substructures, up to the completely closed triazafullerene **2**, could be identified within the layer (Figure 5f). Thus, the layer morphology is not fully flat but bumped. The origin of the height roughness is twofold. On one hand, we have to keep in mind that N atoms are included in the layer and the local density of states at the N sites can be much higher. Second, **1** includes both pentagons and hexagons and, therefore, the precursor should (partially) fold upon (partial) cyclodehydrogenation. As mentioned above, the triangular features are not visible at this temperature, indicating both an almost complete removal of H atoms and an intramolecular recombination process (see Supporting Information).

Phase Diagrams of Dehydrogenation of 4 Mediated by Pt(111), Cu(110), Cu(111), and Au(111) Surfaces. To provide a comprehensive view on the role of the adsorbate–surface interaction and annealing temperature in (cyclo)dehydrogenation of (hetero)aromatic precursors, we constructed a phase diagram for the dehydrogenation of **4** on various single-crystal surfaces by analyzing dozens of STM images (Figure 6). Within a temperature range of 300–825 K intriguing differences emerged in the behavior of the Pt(111) *versus* Cu(110), Cu(111), and Au(111), which were manifested by different phase-transition temperatures and structures of dehydrogenation products.

In the case of Pt(111), where **4** showed no diffusion, two phase transitions can be seen: a conversion of the precursor **4** to diazahexabenzocoronene **5** at a threshold temperature of 580 K (indicated by a narrow transient region between the light green and dark green zones in Figure 6a, column 1) and a transition from the latter to the N-doped graphene layer at 850 K (not shown in the figure).

In sharp contrast to that, **4** diffuses on the coinage metals at RT, hence favoring the conversion of **4** to the polymeric cross-linked networks **6** at the threshold temperature of 550 K for Cu(110), 610 K for Cu(111), and 675 K for Au(111) (Figure 6a, columns 2–4). The second phase transition results in the growth of an N-doped graphene layer,[14,35] as supported by the N1s-XPS (see Supporting Information). The determined threshold temperatures for this N-graphene phase are 665 K for Cu(110) and 775 K for Cu(111) (Figure 6a, columns 2 and 3). We have not observed the formation of N-doped graphene on Au(111) below the upper limit of 825 K (Figure 6a, column 4).

For the coinage metals, the transient regions are about 50 K broad (indicated by a color gradient between the light blue/blue zones or blue/dark blue zones in Figure 6a, columns 2–4). The substrate-dependent transformation of **4** supports the concept of metal catalysis in on-surface dehydrogenation processes. The (110) face of Cu is the most catalytically active in transforming the precursor **4** to N-doped graphene. Actually, the (110) face exhibits close-packed rows of the Cu atoms, which are more reactive and, therefore, dehydrogenation and graphenization reactions are boosted here. Annealing the precursor **1** on different surfaces leads to similar results with moderate differences in transition temperatures of individual phases.

We characterize each phase transition of **4** on copper and gold with NEXAFS recorded at the C K-edge. Upon the deposition and below the first transition temperature, **4** diffuses on copper and gold surfaces, and therefore, molecular resolution cannot be achieved with the STM at RT (Figure 6a, light blue zone in columns 2–4). However, the intense π^* contributions from both the P-polarized beam (the electric field of the X-ray beam was perpendicular to the surface, black curve) and the S-polarized beam (the electric field was parallel to the surface, red curve) in the NEXAFS C K-edge spectrum evidence the presence of **4** on the surface (Figure 6b and Supporting Information). The lack of a complete dichroism of the π^* feature between S- and P-polarized spectra indicates that the molecular adsorbates preserve their natural three-dimensional helical structure upon adsorption when diffusing on the surface (see the model of **4**, Figure 1). In fact, it has to be noticed that the profile of the π^* contribution is slightly different in the two polarizations. This excludes that the limited dichroism depends solely on a possible tilt of the molecule with respect to the surface and suggests that it is due to the contribution of the differently oriented regions of the contorted pristine molecule. Moreover, we observe the same situation on the Cu(111) surface, which excludes that we have here some important effects induced by a particular azimuthal orientation of the molecules, driven by the 2-fold symmetry of the substrate.

After annealing above the threshold temperatures, when the polymeric networks **6** form (Figure 6a, the blue zone in columns 2–4), we observe a strong dichroism of the π^* contribution of the NEXAFS C

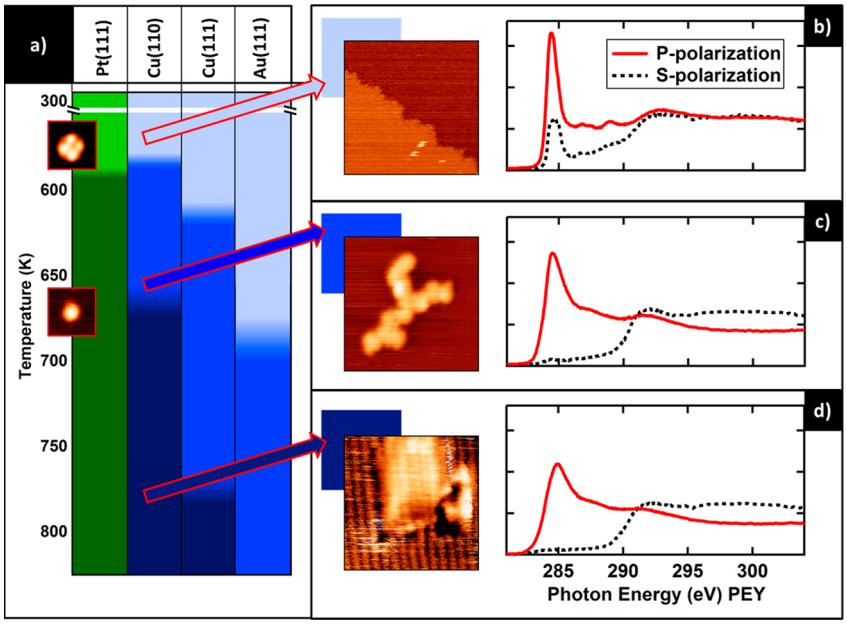

Figure 6. Phase diagrams, STM images, and NEXAFS spectra of the different nanostructures formed by surface-assisted (cyclo)dehydrogenation of 4 on four different single-crystal surfaces, namely, Pt(111), Cu(110), Cu(111), and Au(111), in the range between room temperature and 825 K. (a) The different colors indicate different nanoarchitectures. Column 1 shows 4 deposited on Pt(111) (light green zone), which undergoes one phase transition upon annealing to form azahexabenzocoronene 5 (dark green zone). The insets show the STM images of 4 and, after annealing, 5 (4×4 nm^2; $V_{substrate} = +2$ V). The N-doped graphene grown at 850 K is not shown in column 1. The diffusion of 4 on Cu(110), Cu(111), and Au(111) is indicated by the light blue region in columns 2−4. Upon annealing, after the first transition temperature, the polymeric structure 6 is formed (blue zone in columns 2−4) and, at higher temperature, a N-doped graphene layer (dark blue zone in columns 2 and 3). (b) The light blue zone refers to the freely diffusing molecules 4 (30×30 nm^2; $V_{substrate} = -2$ V). (c) The blue zone refers to the polymeric chains 6 (30×30 nm^2; $V_{substrate} = +2$ V). (d) The dark blue zone refers to the N-doped graphene phase (30×30 nm^2; $V_{substrate} = +2$ V). Next to the STM images b−d, the corresponding C K-edge NEXAFS spectra are presented.

K-edge spectrum for both S- and P-polarizations (Figure 6c). This result indicates that the molecular adsorbates flatten as a result of dehydrogenation (see **6**, Figure 1). Furthermore, the peak at 284.8 eV (corresponding to the C1s transition of the aromatic rings to the π^* unoccupied states in the P-polarized spectrum) becomes significantly broader than that of the diffusing molecules **4** (Figure 6b). A similar spectrum was recorded after the formation of the N-doped graphene layer above the second threshold temperatures (Figure 6d, dark blue zone in columns 2 and 3). The shape and the position of the peaks are consistent with that of graphene,[14,36] while the broadening of the π^* feature upon annealing in relation to that reported for free-standing graphene is due to the flake edges, inclusion of N atoms in the mesh, and possible hybridization with the surface.

CONCLUSIONS

The adsorbate−surface interaction plays a key role in tailoring the outcome of the on-surface dehydrogenation of suitable (hetero)aromatic precursors. Under temperature and substrate control, cyclodehydrogenation and dehydrogenative polymerization compete to govern the on-surface reaction in favor of either individual molecular objects (when their initial diffusion is minimized) or polymeric networks (when diffusion is enhanced). We have found that either (i) a strong coupling of heteroaromatic precursors with the Pt(111) surface blocks the diffusion of molecules and, accordingly, thermally induced intramolecular cyclodehydrogenation dominates or, in contrast, (ii) a weak coupling of heteroaromatic precursors with the Au(111), Cu(110), or Cu(111) surface allows the diffusion of molecules and, therefore, intermolecular dehydrogenative polymerization takes place (along with cyclodehydrogenation). Thus, by using the same heteroaromatic precursor, we can steer the reaction toward the formation of individual molecular nanostructures or complex heteroaromatic networks. Importantly, we demonstrated a straightforward bottom-up approach to nanoscale carbon-rich heteroarchitectures such as azafullerene, azananographene, N-doped polymeric networks, and N-doped carbonaceous overlayers or graphene, which are not accessible by standard tools of chemical synthesis.

METHODS

The experiments were carried out *in situ* in a UHV chamber with a base pressure of 1×10^{-10} mbar. The substrates were carefully cleaned with repeated Ar^+ sputtering and annealing cycles (1150 K for Pt(111), 870 K for Cu(110) and for Cu(111), and 800 K for Au(111)) under UHV conditions. In the case of Pt(111)

two extra annealing cycles under an oxygen atmosphere (1×10^{-7} mbar) were performed. The molecules were deposited from a homemade Ta crucible on the clean surfaces (T_{evap} of **1**: 675 K; T_{evap} of **4**: 570 K), whose temperature was monitored with a type-K thermocouple spot-welded to the Ta. The pressure during evaporation never exceeded 5×10^{-10} mbar. The STM images were recorded in a room-temperature STM in constant current mode. The WSxM program[37] was used for data acquisition and analysis. NEXAFS spectra were measured in the MAX-IV laboratory (Lund, Sweden) using beamline D1011 with linearly polarized light and a photon energy resolution of 80 meV. The sample was held at room temperature, and spectra were recorded by changing the photon incidence angle (P-polarization = 20° and S-polarization = 90°).

For *ab initio* atomistic simulations of **4** on Pt(111), DFT was used effectively, combining the localized-basis-set and plane-wave schemes as implemented in the Fireball[38] and PwScf[39] simulation packages, respectively, accounting for van der Waals corrections in a perturbative framework.[40] We used the PW91 exchange–correlation parametrizations to describe the XC effects[41] and norm-conserving scalar-relativistic pseudopotentials[42] to model the ion–electron interaction. The Pt(111) surface was modeled in a repeated slab geometry: a slab of four Pt(111) layers and a distance ~25 Å in vacuum, with full periodic boundary conditions representing an infinite Pt(111) surface. Each layer contained 64 Pt atoms, and the size of the unit cell in the direction parallel to the surface was 22.5×22.5 Å^2. To define the equilibrium geometries and energies of the different intermediate states of the reaction, we performed full geometry optimizations (only the two bottom Pt layers were kept fixed).

Conflict of Interest: The authors declare no competing financial interest.

Supporting Information Available: Synthesis of precursor **4**; additional STM images of **1** and **3** on Au(111); XPS and NEXAFS of **4**; details of theoretical calculations. This material is available free of charge *via* the Internet at http://pubs.acs.org.

Acknowledgment. We acknowledge financial support by Spanish research projects Nos. MAT2011-26534, CSD2007-41, CTQ2010-18813, and S2009/MAT-1756/CAM, the Czech Science Foundation project No. P207/10/2207, and the Institute of Organic Chemistry and Biochemistry, Academy of Sciences of the Czech Republic (RVO: 61388963). We are grateful to M. Gonzalez and L. Sánchez for their help during image processing and acquisition, respectively.

REFERENCES AND NOTES

1. Wei, D.; Liu, Y. Controllable Synthesis of Graphene and Its Applications. *Adv. Mater.* **2010**, *22*, 3225–3241.
2. Méndez, J.; López, M. F.; Martín-Gago, J. A. On-Surface Synthesis of Cyclic Organic Molecules. *Chem. Soc. Rev.* **2011**, *40*, 4578–4590.
3. Otero, G.; Biddau, G.; Sánchez-Sánchez, C.; Caillard, R.; López, M. F.; Rogero, C.; Palomares, F. J.; Cabello, N.; Basanta, M. A.; Ortega, J.; *et al.* Fullerenes from Aromatic Precursors by Surface-Catalysed Cyclodehydrogenation. *Nature* **2008**, *454*, 865–869.
4. Amsharov, K.; Abdurakhmanova, N.; Stepanow, S.; Rauschenbach, S.; Jansen, M.; Kern, K. Towards the Isomer-Specific Synthesis of Higher Fullerenes and Buckybowls by the Surface-Catalyzed Cyclodehydrogenation of Aromatic Precursors. *Angew. Chem., Int. Ed.* **2010**, *49*, 1–6.
5. Treier, M.; Pignedoli, C. A.; Laino, T.; Rieger, R.; Müllen, K.; Passerone, D.; Fasel, R. Surface-Assisted Cyclodehydrogenation Provides a Synthetic Route towards Easily Processable and Chemically Tailored Nanographenes. *Nat. Chem.* **2011**, *3*, 61–67.
6. Cai, J.; Ruffieux, P.; Jaafar, R.; Bieri, M.; Braun, T.; Blankenburg, S.; Muoth, M.; Seitsonen, A. P.; Saleh, M.; Feng, X.; *et al.* Atomically Precise Bottom-up Fabrication of Graphene Nanoribbons. *Nature* **2010**, *466*, 470–473.
7. Rim, K. T.; Siaj, M.; Xiao, S.; Myers, M.; Carpentier, V. D.; Liu, L.; Su, C.; Steigerwald, M. L.; Hybertsen, M. S.; McBreen, P. H.; *et al.* Forming Aromatic Hemispheres on Transition-Metal Surfaces. *Angew. Chem., Int. Ed.* **2007**, *46*, 7891–7895.
8. Grill, L.; Dyer, M.; Lafferentz, L.; Persson, M.; Peters, M. V; Hecht, S. Nano-Achitectures by Covalent Assembly of Molecular Building Blocks. *Nat. Nanotechnol.* **2007**, *2*, 687–691.
9. Lafferentz, L.; Eberhardt, V.; Dri, C.; Africh, C.; Comelli, G.; Esch, F.; Hecht, S.; Grill, L. Controlling On-Surface Polymerization by Hierarchical and Substrate-Directed Growth. *Nat. Chem.* **2012**, *4*, 215–220.
10. Lipton-Duffin, J. A.; Ivasenko, O.; Perepichka, D. F.; Rosei, F. Synthesis of Polyphenylene Molecular Wires by Surface-Confined Polymerization. *Small* **2009**, *5*, 592–759.
11. Lafferentz, L.; Ample, F.; Yu, H.; Hecht, S.; Joachim, C.; Grill, L. Conductance of a Single Conjugated Polymer as a Continuous Function of Its Length. *Science* **2009**, *323*, 1193–1198.
12. Bieri, M.; Nguyen, M.; Gro, O.; Cai, J.; Treier, M.; At-Mansour, K.; Ruffieux, P.; Pignedoli, C. A.; Passerone, D.; Kastler, M.; *et al.* Two-Dimensional Polymer Formation on Surfaces: Insight into the Roles of Precursor Mobility and Reactivity. *J. Am. Chem. Soc.* **2010**, *132*, 16669–16676.
13. Kittelmann, M.; Rahe, P.; Nimmrich, M.; Hauke, C. M.; Ku, A. On-Surface Covalent Linking of Organic Building Blocks on a Bulk Insulator. *ACS Nano* **2011**, *5*, 8420–8425.
14. Usachov, D.; Vilkov, O.; Grüneis, A.; Haberer, D.; Fedorov, A.; Adamchuk, V. K.; Preobrajenski, A. B.; Dudin, P.; Barinov, A.; Oehzelt, M.; *et al.* Nitrogen-Doped Graphene: Efficient Growth, Structure, and Electronic Properties. *Nano Lett.* **2011**, *11*, 5401–5407.
15. Gourdon, A. On-Surface Covalent Coupling in Ultrahigh Vacuum. *Angew. Chem., Int. Ed.* **2008**, *47*, 6950–6953.
16. Bartels, L. Tailoring Molecular Layers at Metal Surfaces. *Nat. Chem.* **2010**, *2*, 87–95.
17. Franc, G.; Gourdon, A. Covalent Networks through On-Surface Chemistry in Ultra-High Vacuum: State-of-the-Art and Recent Developments. *Phys. Chem. Chem. Phys.* **2011**, *13*, 14283–14292.
18. Lackinger, M.; Heckl, W. M. A STM Perspective on Covalent Intermolecular Coupling Reactions on Surfaces. *J. Phys. D: Appl. Phys.* **2011**, *44*, 1–14.
19. Palma, C. A.; Samorì, P. Blueprinting Macromolecular Electronics. *Nat. Chem.* **2011**, *3*, 431–436.
20. In't Veld, M.; Iavicoli, P.; Haq, S.; Amabilino, D. B.; Raval, R. Unique Intermolecular Reaction of Simple Porphyrins at a Metal Surface Gives Covalent Nanostructures. *Chem. Commun.* **2008**, 1536–1538.
21. Zhong, D.; Franke, J.-H.; Podiyanachari, S. K.; Blömker, T.; Zhang, H.; Kehr, G.; Erker, G.; Fuchs, H.; Chi, L. Linear Alkane Polymerization on a Gold Surface. *Science* **2011**, *334*, 213–216.
22. Matena, M.; Riehm, T.; Stöhr, M.; Jung, T. A.; Gade, L. H. Transforming Surface Coordination Polymers into Covalent Surface Polymers: Linked Polycondensed Aromatics through Oligomerization of N-Heterocyclic Carbene Intermediates. *Angew. Chem., Int. Ed.* **2008**, *47*, 2414–2417.
23. Kanuru, V. K.; Kyriakou, G.; Beaumont, S. K.; Papageorgiou, A. C.; Watson, D. J.; Lambert, R. M. Sonogashira Coupling on an Extended Gold Surface in Vacuo: Reaction of Phenylacetylene with Iodobenzene on Au(111). *J. Am. Chem. Soc.* **2010**, *132*, 8081–8086.
24. Lipton-Duffin, J. A.; Miwa, J. A.; Kondratenko, M.; Cicoira, F.; Sumpter, B. G.; Meunier, V.; Perepichka, D. F.; Rosei, F. Step-by-Step Growth of Epitaxially Aligned Polythiophene by Surface-Confined Reaction. *P. Natl. Acad. Sci. U.S.A.* **2010**, *107*, 11200–11204.
25. Gutzler, R.; Walch, H.; Eder, G.; Kloft, S.; Heckl, W. M.; Lackinger, M. Surface Mediated Synthesis of 2D Covalent Organic Frameworks: 1,3,5-Tris(4-bromophenyl)benzene on Graphite(001), Cu(111), and Ag(110). *Chem. Commun.* **2009**, 4456–4458.
26. Gómez-Lor, B.; Echavarren, A. M. Synthesis of a Triaza Analogue of Crushed-Fullerene by Intramolecular Palladium-Catalyzed Arylation. *Org. Lett.* **2004**, *6*, 2993–2996.

27. Jančařík, A.; Stará, I. G.; Starý, I. To be published.
28. Violi, A. Cyclodehydrogenation Reactions to Cyclopenta-fused Polycyclic Aromatic Hydrocarbons. *J. Phys. Chem. A* **2005**, *109*, 7781–7787.
29. Otero, G.; Biddau, G.; Ozaki, T.; Gómez-Lor, B.; Méndez, J.; Pérez, R.; Martín-Gago, J. A. Spontaneous Discrimination of Polycyclic Aromatic Hydrocarbon (PAH) Enantiomers on a Metal Surface. *Chem.—Eur. J.* **2010**, *16*, 13920–13924.
30. Liu, C.; Qin, Z.; Chen, J.; Guo, Q.; Yu, Y.; Cao, G. Molecular Orientations and Interfacial Structure of C60 on Pt(111). *J. Chem. Phys.* **2011**, *134*, 164707.
31. Weiss, K.; Beernink, G.; Dötz, F.; Birkner, A.; Müllen, K.; Wöll, C. Template-Mediated Synthesis of Polycyclic Aromatic Hydrocarbons: Cyclodehydrogenation and Planarization of a Hexaphenylbenzene Derivative at a Copper Surface. *Angew. Chem., Int. Ed.* **1999**, *38*, 3748–3752.
32. Beernink, G.; Gunia, M.; Dötz, F.; Öström, H.; Weiss, K.; Müllen, K.; Wöll, C. Synthesis of Polycyclic Aromatic Hydrocarbons and Graphite Islands *via* Surface-Induced Reaction of Small Molecules. *ChemPhysChem* **2001**, *2*, 317–320.
33. Henkelman, G.; Uberuaga, B. P.; Jónsson, H. A Climbing Image Nudged Elastic Band Method for Finding Saddle Points and Minimum Energy Paths. *J. Chem. Phys.* **2000**, *113*, 9901–9904.
34. Martínez-Galera, A. J.; Brihuega, I.; Gómez-Rodríguez, J. M. Ethylene Irradiation: A New Route to Grow Graphene on Low Reactivity Metals. *Nano Lett.* **2011**, *11*, 3576–3580.
35. Wang, H.; Maiyalagan, T.; Wang, X. Review on Recent Progress in Nitrogen-Doped Graphene: Synthesis, Characterization, and Its Potential Applications. *ACS Catal.* **2012**, *2*, 781–794.
36. Preobrajenski, A. B.; Ng, M. L.; Vinogradov, A. S.; Mårtensson, N. Controlling Graphene Corrugation on Lattice-Mismatched Substrates. *Phys. Rev. B* **2008**, *78*, 2–5.
37. Horcas, I.; Fernández, R.; Gómez-Rodríguez, J. M.; Colchero, J.; Gómez-Herrero, J.; Baro, a M. WSXM: A Software for Scanning Probe Microscopy and a Tool for Nanotechnology. *Rev. Sci. Instrum.* **2007**, *78*, 013705.
38. Lewis, J. P.; Jelínek, P.; Ortega, J.; Demkov, A. A.; Trabada, D. G.; Haycock, B.; Wang, H.; Adams, G.; Tomfohr, J. K.; Abad, E.; *et al*. Advances and Applications in the FIREBALL ab Initio Tight-Binding Molecular-Dynamics Formalism. *Phys. Status Solidi B* **2011**, *248*, 1989–2007.
39. Baroni, S.; Corso, A. D.; De Gironcoli, S.; Giannozzi, P. QUANTUMESPRESSO package, www.quantum-espresso.org.
40. Abad, E.; Dappe, Y. J.; Martínez, J. I.; Flores, F.; Ortega, J. C6H6/Au(111): Interface Dipoles, Band Alignment, Charging Energy, and van der Waals Interaction. *J. Chem. Phys.* **2011**, *134*, 044701.
41. Perdew, J. P.; Jackson, K. A.; Pederson, M. R.; Singh, D. J.; Fiolhais, C. Atoms, Molecules, Solids and Surfaces: Applications of the Generalized Gradient Approximation for Exchange and Correlation. *Phys. Rev. B* **1992**, *46*, 6671–6687.
42. Vanderbilt, D. Soft Self-Consistent Pseudopotentials in a Generalized Eigenvalue Formalism. *Phys. Rev. B* **1986**, *41*, 7892–7895.